analytical chemistry

pubs.acs.org/ac Article

Weak Anion-Exchange Chromatography Coupled with FT-ICR MS Resolves Polarity-Driven Molecular Signatures in Natural and Anthropogenic Dissolved Organic Matter

Joseph W. Frye-Jones, Lissa C. Anderson, Winston K. Robbins, Germain Salvato Vallverdu, Alvaro J. Tello Rodriguez, Mason C. Hagan, Alan G. Marshall, Brice Bouyssiere, Pierre Giusti, Ryan P. Rodgers, and Martha L. Aguilera*

Cite This: *Anal. Chem.* 2026, 98, 601−610 Read Online

ACCESS | Metrics & More | Article Recommendations | Supporting Information

ABSTRACT: Water-soluble emerging contaminants from fossil fuel−based materials pose increasing environmental risks, yet their detailed molecular characterization remains limited. These compounds often resemble natural dissolved organic matter (DOM), especially after photo-oxidation, which increases oxygen content and structural complexity. We developed a high-performance liquid chromatography (HPLC) method coupled to 21 T Fourier-transform ion cyclotron resonance mass spectrometry (FT-ICR MS) to enhance molecular analysis of both natural and anthropogenic DOM. The method incorporates a polymeric stationary phase functionalized with amine groups to promote interactions with carboxylic and phenolic moieties. A methanol-to-water gradient containing 2% diethylamine (DEA) promotes separation based on differences in hydrophilicity and functional group interactions with the stationary phase. Compared with direct infusion (DI), the HPLC-FT-ICR MS workflow mitigates ion suppression, enhances ionization efficiency, and broadens molecular coverage. For example, analysis of coal tar−derived water solubles yielded over 16,000 assigned formulas, twice as many as in DI-MS, including oxygen-containing polycyclic aromatic hydrocarbons (oxy-PAHs) and high H/C species poorly ionized under DI conditions. This method achieves efficient separation of chemically diverse compound classes, enabling ultrahigh-resolution MS analysis of complex environmental mixtures and advancing molecular-level understanding of both natural DOM and fossil fuel−derived contaminants.

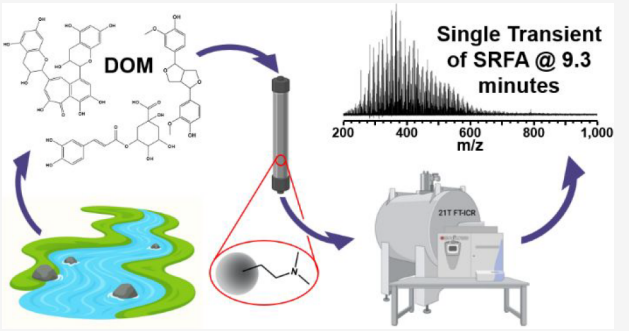

INTRODUCTION

Natural organic matter (NOM) is ubiquitous in aquatic systems, where it influences nutrient cycling, carbon transport, and ecosystem stability. Formed through the degradation of plant and microbial biomass, NOM contains bioactive compounds that affect water quality and ecological function. Its soluble fraction, dissolved organic matter (DOM), contains thousands of chemically diverse species, including humic substances, carbohydrates, and amino acids, whose complexity presents major analytical challenges.

Fossil fuel−derived dissolved organic carbon (DOC) shares many molecular features with natural DOM, especially as photooxidation increases oxygen content and structural heterogeneity.[1] These materials enter aquatic environments via oil spills, urban runoff, and other anthropogenic inputs, increasing the chemical diversity of water-soluble organic matter in affected ecosystems.[2,3] Understanding the molecular similarities and distinctions between natural DOM and fossil fuel−derived contaminants is essential for accurate environmental risk assessment.

Water-soluble contaminants produced by photooxidation of fossil fuel−derived materials pose persistent health and environmental risks. Weathered in aquatic and urban settings, these compounds are often more toxic than their precursor hydrocarbons. Their high solubility enhances the mobility and bioavailability of metals and polycyclic aromatic hydrocarbons (PAHs).[4,5] Urban sources such as asphalt binders and pavement sealants release oxidized PAHs (oxy-PAHs) that leach into waterways and contribute to long-term contamination.[6,7] Although structurally similar to natural DOM, these compounds introduce distinct environmental hazards, reinforcing the need for robust analytical methods to characterize their composition and transformation products.

Received: September 8, 2025
Revised: November 12, 2025
Accepted: November 20, 2025
Published: December 22, 2025

https://doi.org/10.1021/acs.analchem.5c05562
Anal. Chem. 2026, 98, 601−610

Ultrahigh-resolution mass spectrometry, e.g., 21 tesla (T) Fourier-transform ion cyclotron resonance (FT-ICR MS), is essential for characterizing the molecular complexity of DOM.[8−13] Analyses of standards such as Suwannee River fulvic acid (SRFA) have revealed up to ∼36,000 unique molecular formulas, spanning aliphatic to highly aromatic compounds with varied heteroatom content. The 21 T FT-ICR MS system resolves isotopic fine structure and isobaric species differing by as little as 0.430 mDa, providing the mass measurement accuracy and resolution needed to profile both natural and fossil fuel−derived DOM at the molecular level.[13] However, several benefits of FT-ICR MS are offset in direct infusion (DI) analysis by ion suppression.[14] In DI-MS, highly abundant, easily ionized compounds can suppress ionization of less abundant species during electrospray ionization (ESI), which limits or prevents their detection.[15−17] This effect is pronounced in DOM, where low-molecular-weight compounds often mask higher-mass or more functionalized molecules. DI-MS also lacks the ability to distinguish isomers, limiting structural and functional interpretation.

The work herein demonstrates that coupling weak anion-exchange chromatography to ultrahigh-resolution FT-ICR MS resolves polarity-driven compositional trends in dissolved organic matter from both natural and anthropogenic sources, establishing a framework to directly compare molecular distributions obtained by HPLC-MS and DI-MS. Coupling HPLC with FT-ICR MS improves molecular coverage via time-resolved separation, thereby minimizing ion suppression.[18] In this context, complex mixtures are separated based on polarity and functional group chemistry, which increases the detection of low-abundance species. For example, a recent reversed-phase HPLC high-resolution mass spectrometry (HRMS) study demonstrated its effectiveness for characterizing water samples from diverse sources, assigning ∼14,000 molecular formulas in both (+) and (−) ESI. In comparison, DI analysis using the same ionization conditions yielded only about 5,000 molecular assignments.[19] Other recent studies with higher-resolution FT-ICR MS have demonstrated excellent reproducibility and broader DOM coverage, with more than ∼14,000 molecular formulas assigned per marine sample.[20,21] Together, these findings highlight the ability of HPLC-FT-ICR MS to access chemical diversity that remains undetected by DI-MS.

This study introduces an HPLC method optimized for coupling with negative-ion ESI 21 T FT-ICR MS to improve the molecular characterization of both natural DOM and water-soluble emerging contaminants. The method relies on a polymeric stationary phase functionalized with dimethylaminopropyl groups, which interact with acidic moieties such as carboxylic acids and phenols through weak anion-exchange interactions and hydrogen bonding. The gradient transitions from methanol to water with 2% diethylamine (DEA), enabling separation based on acidity, polarity, and hydrophilicity. This dual-mode mechanism allows efficient elution of structurally diverse species, including low-abundance aliphatic molecules, polyaromatics, and highly functionalized compounds often missed by DI-MS or conventional reversed-phase separations. When combined with ultrahigh-resolution mass spectrometry and advanced data processing, this workflow expands molecular coverage and reveals compound families not accessible through DI-MS alone.

METHODS

Materials

Fulvic and humic acid standards, including Suwannee River isolates, were obtained from the International Humic Substances Society. Water-soluble compounds derived from fossil fuel−based materials were prepared through the photooxidation of coal tar sealant and coal C_7 asphaltenes, following established protocols.[22] Model compounds with diverse oxygen-containing functional groups were purchased from MilliporeSigma. Detailed information about solvents, standards, samples, and stationary phase materials is provided in the Supporting Information (Section S1).

Offline Solid-Phase Extraction (SPE) and Online HPLC Separations

Initial method development was conducted offline using solid-phase extraction (SPE) with POROS GoPure 50 D resin functionalized with dimethylaminopropyl groups (Thermo Fisher Scientific). DOM standards and fossil fuel−derived samples were fractionated using a methanol-to-aqueous diethylamine (DEA) gradient provided in the Supporting Information (Section S1, Table S2/S3). These results informed the design of an online HPLC method employing a prepacked POROS GoPure 50 D column coupled to a Waters Corporation Alliance e2695 separation module and a Waters 2998 photodiode array (PDA) detector.

The optimized gradient incorporated methanol and water with 2−5% DEA (v/v), enabling an initial separation driven by weak anion-exchange interactions followed by partitioning and hydrogen-bonding effects. Gradient conditions, flow rates, and eluent compositions are provided in the Supporting Information (Section S1, Table S4). Method performance was evaluated using model compounds and DOM standards, analyzed individually, in mixtures, and in spiked combinations. Reproducibility was confirmed by alignment of PDA chromatograms across repeated injections, which showed consistent retention times and identical elution behaviors throughout the runs.

FTMS Characterization

DOM standards and fossil fuel−derived samples were analyzed on a custom-built 21 T FT-ICR MS using negative-ion heated electrospray ionization (HESI).[23] Both direct infusion and HPLC-coupled experiments were performed. Model compounds were characterized on a Thermo Fisher Scientific Orbitrap Eclipse™ Tribrid™ MS instrument under similar ionization conditions. For HPLC-MS, the PDA detector effluent was split before introduction into the electrospray ion source. Instrument settings, acquisition parameters, and calibration procedures are provided in the Supporting Information (Section S1). Data processing was carried out using Predator, PetroOrg, and PyC2MC for FT-ICR MS, and Xcalibur™ for Orbitrap MS analyses.[24−26] Molecular formulas were assigned using PetroOrg for segmented spectra and both PetroOrg and PyC2MC for individual spectra. Custom Python scripts were used to organize the assigned formulas, extract compositional parameters (DBE, O/C, H/C), and generate custom chromatograms and abundance-weighted profiles for direct comparison between HPLC and DI data sets. Ionization behavior was evaluated based on relative signal intensity and the injection times required to accumulate $\sim 2 \times 10^6$ charges per scan, with longer injection times observed for fractions

https://doi.org/10.1021/acs.analchem.5c05562
Anal. Chem. 2026, 98, 601−610

exhibiting lower ionization efficiency, similar to trends reported for other complex mixtures, e.g., asphaltenes.

RESULTS

The results integrate the chromatographic behavior of model compounds with FT-ICR MS characterization of complex DOM, revealing how weak anion-exchange HPLC-MS uncovers polarity-dependent compositional trends that remain obscured in DI analyses.

Efforts to improve DOM separations were motivated by prior work on fossil fuels, where fractionating acidic species substantially increased FT-ICR MS coverage.[27] We aimed to apply this approach to DOM, but its polyfunctional nature presents challenges not encountered with petroleum acids. Aminopropyl silica (APS) gel and other silica-based stationary phases, although effective for fossil fuel acids, are poorly suited for DOM. Strong interactions with silica surfaces (e.g., SiO_2) hinder desorption and reduce recovery. Although acidic conditions effectively elute petroleum acids, DOM requires desorption at high pH, which destabilizes the silica gel, limiting compatibility with online HPLC-MS.

Initial tests with APS gel used a methanol−water gradient, where the pH of the aqueous phase was adjusted to 11 with ammonium hydroxide. As previously reported and shown in Figure S1a, this approach failed due to silica particle migration and irreversible sample binding.[28] Substituting ammonium hydroxide with 2% diethylamine (DEA) improved the recovery but did not fully resolve these issues.

To address these limitations, we adopted a polymeric stationary phase composed of poly(styrene−co−divinylbenzene) functionalized with dimethylaminopropyl groups, hereafter referred to as POROS. Unlike silica-based materials, polymeric particles remain stable at high pH and separate both hydrophobic and hydrophilic DOM species through multiple interactions. Offline SPE using 2% DEA with POROS achieved a 98% recovery. This demonstrates substantially reduced irreversible adsorption (Figure S1b).

SPE fractions were analyzed by DI-FT-ICR MS, and the results were visualized as van Krevelen diagrams (Figure S1c). Molecular formulas are plotted by their H/C and O/C ratios, with relative abundance indicated by color gradient. In the 2% DEA experiment, the first fraction (upper row, Figure S1c) was dominated by aliphatic, hydrogen-rich species with low oxygen content. Fraction 2 exhibited broader compositional diversity, whereas Fraction 3 was enriched in highly aromatic compounds with variable oxygen content. No additional material eluted beyond Fraction 3. Thus, to extend the separation, the DEA concentration was reduced to 1%, yielding six distinct fractions.

Van Krevelen diagrams from the 1% DEA separation (Figure S1c, middle row) revealed a similar progression, with a shift from aliphatic to increasingly aromatic and oxygen-rich species across Fractions 1−6. Figure S1b shows the physical appearance of these fractions, each diluted to 5000 ppm in 80:20 methanol:water. The observed color differences reflect the underlying compositional variation. Importantly, ion injection times required to accumulate 2×10^6 charges increased markedly across the gradient, from 0.3−3 s across Fractions 1−6, which suggests that nanoaggregation in later fractions reduced ionization efficiency.

Decreased ionization efficiency in the latter fractions likely reflects contributions from two effects. First, a stronger intermolecular association is consistent with our experimental observations, including repeated electrospray emitter clogging and the need to switch from nano-ESI to HESI for stable operation, which mirrors behavior reported for complex mixtures with strong aggregation tendencies such as asphaltenes.[29−31] Second, increased polarity can lower the electrospray response by reducing surface activity and altering charge competition during droplet fission, thereby decreasing ion yield. Both factors likely contribute to the observed decrease in signal.[32]

To improve the resolution further, the DEA concentration was lowered to 0.5%. This adjustment enhanced the separation, particularly in early fractions. Fractions 1−3 captured a clear transition from aliphatic to aromatic species, whereas later fractions retained high aromaticity but exhibited a broader O/C range. For the most abundant species, the shift from oxygen-rich to oxygen-depleted structures was most evident in Fraction 6.

The successful separations achieved with 1% and 0.5% DEA provided the basis for adapting the method to an online HPLC-FT-ICR MS configuration using a commercially available POROS column. Importantly, the improved elution scheme with lower DEA concentration increased the resolution between early- and late-eluting fractions, yielding a progressive transition from more aliphatic to more aromatic molecular compositions (Figure S1c, bottom row). In this context, gradient optimization was critical to achieving complete elution and maximizing molecular coverage. Initial tests with 0.5% DEA led to poor separation, with a significant portion of the material retained on the column. Increasing the concentration to 2% DEA improved the elution efficiency and substantially enhanced the compositional recovery. Based on these optimizations, the final gradient, shown in Figure 1a, was applied to all sample types and enabled broad molecular separation.

The HPLC system includes a photodiode array (PDA) detector positioned upstream of the flow split to the mass spectrometer. Absorbance was recorded at 210−600 nm. PDA chromatograms extracted at 300 nm (Figure 1b) show an early breakthrough peak at ∼2 min, corresponding to methanol-soluble species not retained by the column. Retention profiles beyond this point vary by the sample.

Suwannee River fulvic and humic acids reveal early peaks (zoomed regions in Figure 1b), consistent with nonacidic, unretained compounds. This is followed by a second major elution beginning around 10 min, when the mobile phase reaches ∼20% water with 2% DEA, indicative of strongly retained, highly acidic species. Figure S2 shows the PDA chromatogram for Pahokee Peat fulvic acid, which follows a similar elution trend.

Coal-related materials produce broader, more complex PDA traces, reflecting contributions from both acidic and nonacidic components. The extended elution window suggests a greater functional group diversity. The coal tar−derived water-soluble fraction shows a dominant early peak at ∼2 min, similar to the fulvic and humic acids but in much higher abundance, indicating a large proportion of nonacidic compounds. This aligns with photooxidized PAHs, known to occur in weathered coal tar sealants, bearing ketones rather than carboxylic acids.[6] The PDA response provides information not only on acidity but also on hydrophilicity, since the gradient shifts from less polar to highly polar elution conditions. The sustained absorbance in this region indicates that strongly hydrophilic, oxygen-rich compounds with light-absorbing chromophores

https://doi.org/10.1021/acs.analchem.5c05562
Anal. Chem. 2026, 98, 601−610

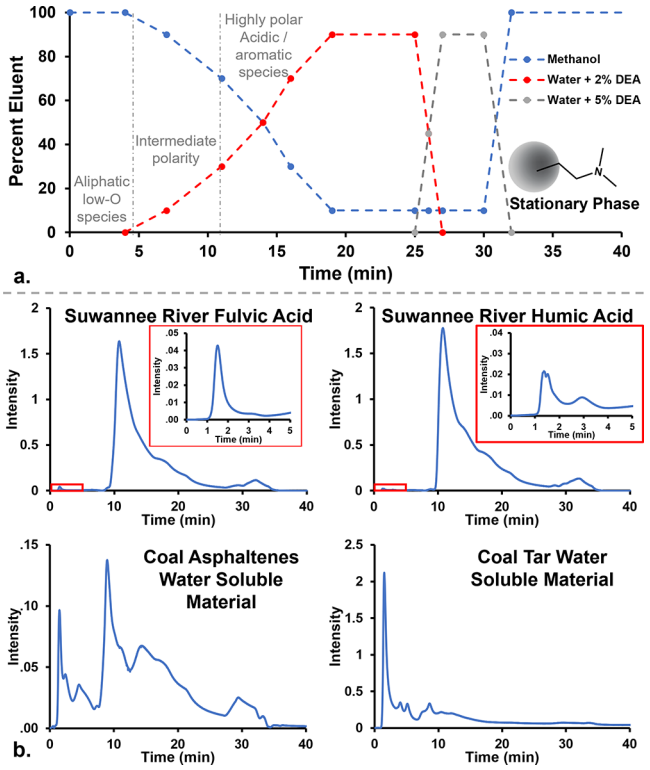

Figure 1. (a) HPLC gradient showing the eluent composition over time for methanol (blue), water with 2% DEA (red), and water with 5% DEA (gray). (b) PDA chromatograms at 300 nm for Suwannee River fulvic and humic acids, and water-soluble species derived from coal asphaltenes and coal tar. Insets highlight early methanol-soluble species in the DOM standards.

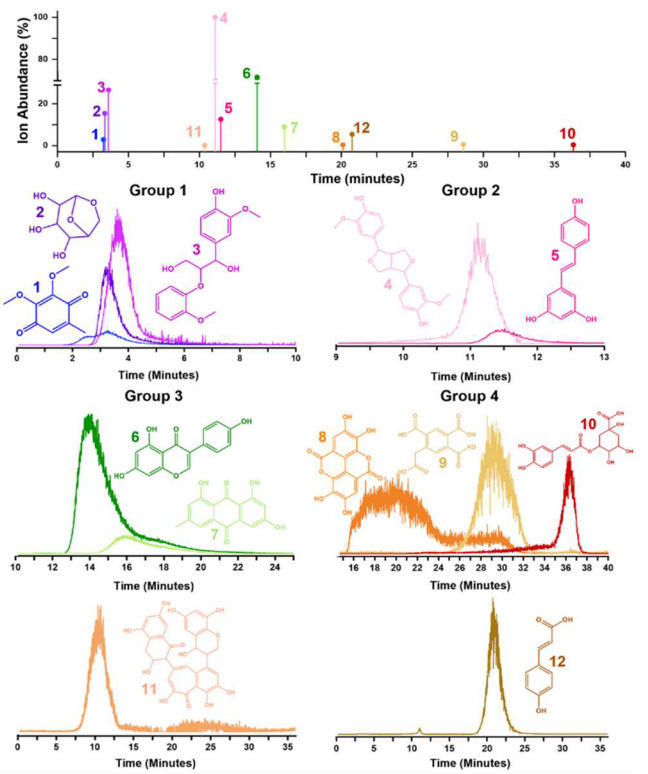

Figure 2. Top panel: Retention times for 12 model compounds analyzed by HPLC negative-ion ESI with Orbitrap MS detection, colored by group. Lower panels: Extracted ion chromatograms (EICs) organized by structural and functional characteristics to highlight differences in acidity, conjugation, and retention behavior under the optimized HPLC conditions. Model compound experiments were performed on an Orbitrap Eclipse mass spectrometer to refine chromatographic conditions prior to 21T FT-ICR MS analyses. Because the mixtures examined here were relatively simple, ultrahigh resolving power was not required, and the Orbitrap provided sufficient mass accuracy and throughput for method development.

are efficiently eluted and detected under these high-polarity conditions.

A set of model compounds with varied oxygen-containing functional groups (Table S1) was used to evaluate retention mechanisms under the optimized HPLC conditions. Their elution profiles (Figure 2) reflect differences in acidity, aromaticity, and interaction with the stationary phase. The data are represented by the centroids of the chromatographic peaks. Group 1 includes compounds with minimal retention, eluting near the methanol front. Compound 1, with negligible acidity, elutes first. Compound 2, which contains nonaromatic hydroxyls, shows slightly greater retention due to its mild acidity. Compound 3, which contains three hydroxyl groups including one phenolic OH, elutes later, consistent with the greater acidity imparted by the phenolic functionality.

Group 2 compares two polyphenolic compounds. Compound 4 has two phenols that are spatially separated, which limits conjugation and reduces acidity. Compound 5 contains three conjugated phenols, leading to greater acidity and increased retention. These results highlight the influence of both the number and spatial arrangement of acidic groups on the retention behavior.

Group 3 consists of two isomers with identical formulas but different electronic environments. Compound 6 elutes earlier, with weakly acidic, nonconjugated phenols. Compound 7 features resonance-stabilized phenols, resulting in stronger retention.

Group 4 includes highly functionalized molecules. Compound 8 contains four phenols and two esters, which were retained moderately via hydrogen bonding and dipolar interactions. Compound 9, a tetracarboxylic acid on an aromatic ring, is strongly retained due to its high acidity and multiple ion-pairing interactions. Compound 10, with phenols, hydroxyls, an ester, and a carboxylic acid, elutes last, reflecting the strongest overall interaction with the stationary phase.

Compound 11 behaves as an outlier. Despite multiple phenolic and hydroxyl groups, it eluted earlier than expected. Its weak retention may result from limited interaction with the stationary phase due to steric hindrance or ineffective ion-exchange interactions rather than pore exclusion. The polymeric material has large pores, making exclusion unlikely for molecules of this size. The chromatogram shows low-abundance delayed-elution peaks, consistent with partial retention. In contrast, Compound 12, a smaller molecule with a single phenol and carboxylic acid, shows strong retention, reflecting efficient interaction with the stationary phase that is not hindered by steric effects.

The model compound results confirm that the elution order is primarily governed by the acidity of oxygen-bound protons and the degree of conjugation. These elution patterns reflect a separation mechanism primarily governed by weak anion-exchange and hydrogen bonding interactions. The addition of a weak base, diethylamine, competes for acidic analytes to interact with the amino groups of the stationary phase. By simple mass action, DEA intercepts acids in the mobile phase,

https://doi.org/10.1021/acs.analchem.5c05562
Anal. Chem. 2026, 98, 601−610

effectively suppressing weak anion-exchange behavior and shifting retention toward partitioning and hydrogen bonding. The HPLC approach relies on functional group interactions between analytes and the dimethylaminopropyl-functionalized stationary phase, offering a retention mode distinct from the hydrophobic interactions used in conventional C18 columns.

Approximate pK_a values for the model compounds are provided in Table S5. These parameters further illustrate that, at the high-pH mobile phase used here, compounds with lower pK_a are retained longer on the weak anion-exchange stationary phase, consistent with the proposed mechanism in which increasing acidity and hydrophilicity govern elution order.

Changes in the mobile phase composition directly influence analyte partitioning by modulating the solvent polarity and analyte ionization. At the beginning of the separation, the high methanol content and nonprotonated amines in the stationary phase minimize ionic interactions, allowing neutral and weakly acidic species to elute with the methanol front while acidic compounds remain bound. As the concentrations of water and diethylamine increase, the rising polarity and base strength promote deprotonation of acidic analytes and their interaction with diethylamine in the mobile phase, which weakens their retention on the anion-exchange sites and facilitates elution.

Comparison across compound groups reveals consistent retention trends governed by functional group acidity, conjugation, and overall functionalization. Weakly acidic, nonconjugated compounds elute near the methanol front, whereas strongly acidic and polyfunctional species are retained longer. These results confirm that retention is primarily driven by the number, strength, and arrangement of the acidic groups. Similar trends are expected in complex mixtures: nonacidic compounds should elute early, mildly acidic species at intermediate retention times, and highly acidic molecules later in the gradient. When identical molecular formulas appear at multiple retention times, they likely represent structural isomers that differ in functional group chemistry.

Complex Mixture Analysis by HPLC-MS

With the elution behavior of model compounds established, the method was applied to complex mixtures, including DOM standards and water-soluble emerging contaminants derived from photoirradiated fossil fuel products. Figures 3 and S3−S5 present extracted ion chromatograms (EICs) from m/z 175−1200, with dominant contaminant peaks removed to facilitate comparison across samples. The ion signal first appears at ∼2 to 3 min, which corresponds to methanol-soluble species not retained by the column. These early eluting compounds ionize efficiently and produce a high-abundance signal that aligns with the first peak in the PDA chromatograms, albeit at a lower relative intensity.

Signal remains stable throughout the high-methanol phase, as methanol lowers the surface tension and enhances electrospray ionization. As the mobile phase shifts to water with 2% DEA, signal intensity drops and approaches zero between 20−28 min. This decline reflects reduced ESI efficiency under highly aqueous and alkaline conditions, rather than an absence of eluting species.[33] A secondary signal increase occurs during the reconditioning phase, as strongly retained compounds elute. Each run was followed by a 10 min reconditioning step (not shown in the EICs) to restore the initial column conditions and maintain reproducibility.

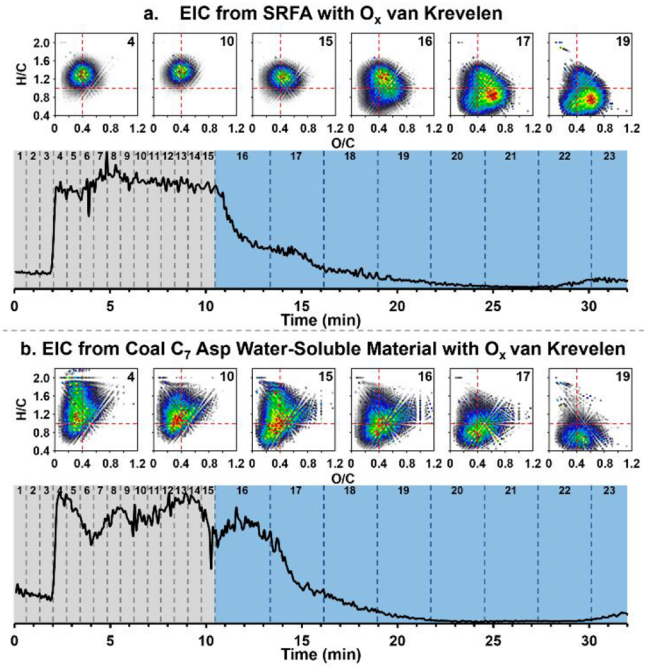

Figure 3. Extracted ion chromatograms (EICs) with corresponding van Krevelen diagrams (O_x classes) at selected time segments for (a) SRFA and (b) coal C_7 asphaltenes water-solubles. Both profiles reveal a compositional transition from aliphatic, low-oxygen species to aromatic, oxygen-rich compounds across the chromatographic gradient. Segment colors in the chromatograms represent the retention time segments used for data segmentation: gray for the first 15 segments, where nine transients were coadded per segment, and blue for the later segments, where 36 transients were coadded to improve the signal-to-noise ratio. In the corresponding van Krevelen diagrams, the color scale represents the normalized relative ion abundance, with red indicating the most abundant compositions, illustrating compositional and abundance shifts across the chromatographic gradient.

Spectral Processing and Analysis

Spectra were processed using a segmentation strategy based on the ion injection times (Figure 3). During the initial ∼10 min of the run, when injection times were short, data were divided into short segments, each composed of nine coadded transients (gray region). The remainder of the run was divided into longer segments, with 36 transients coadded per segment (blue region). The final segment (segment 23) captured any remaining data at the end of the run. Each segment was calibrated using Predator, and molecular formulas were assigned with PetroOrg. Select van Krevelen diagrams were generated for oxygen-containing species (O_x classes) and overlaid on each extracted ion chromatogram (EIC). Red-dashed lines at H/C = 1 and O/C = 0.4 serve as a visual reference to track compositional shifts.

Segment 4 corresponds to the methanol-soluble fraction, which contains compounds that do not interact with the column. Segment 10 marks the onset of elution for more strongly retained species, as water with 2% DEA (solvent B) enters the system. After segment 15, solvent B exceeds 30%, and EIC intensity drops due to reduced ionization efficiency. This trend continues through segments 17−20, where more hydrophilic species elute as the gradient advances.

In SRFA (Figure 3a), the van Krevelen diagrams show a broad compositional shift across the chromatographic run. In

https://doi.org/10.1021/acs.analchem.5c05562
Anal. Chem. 2026, 98, 601−610

segment 4, H/C ratios range from 0.8 to 1.8. By segment 19, H/C values decrease to approximately 0.4, indicating higher aromaticity. O/C ratios follow a similar trend, expanding from 0.1−0.7 in segment 4 to 0.1−0.9 in segment 19. The most abundant species shift from the upper left quadrant (aliphatic, low-oxygen) to the lower right (aromatic, oxygen-rich). Comparison of segments 15, 16, and 17 reveals a subtle drift of the distribution toward the lower left quadrant, reflecting an increase in average molecular weight and aromatic character rather than a loss of oxygen content. Later-eluting species exhibit comparable oxygen content but contain more carbon atoms, leading to lower O/C and H/C ratios consistent with enrichment in larger, more aromatic molecules.

In contrast, the coal-derived, water-soluble material (Figure 3b) shows a broader initial compositional range. In segment 4, H/C ranges from 0.6 to 2.1, and O/C from 0.1 to 0.9. While SRFA shows major compositional shifts beginning around segment 15, the coal-derived sample begins to trend toward the aromatic region (H/C < 1) as early as segment 10. By segments 15−16, a secondary distribution emerges at higher oxygen content (O/C > 0.8). Segment 16 displays a distinct linear cluster at O/C = 1, consistent with highly polar, hydrophilic species, likely polyfunctional, carboxylic-rich compounds. This segment also exhibits the broadest composition, with H/C values from 0.4 to 2.0 and O/C from 0.1 to 1.2. In later segments, van Krevelen diagrams reveal a predominance of highly aromatic species (H/C < 1.0) with a wide range of oxygen content, mirroring the elution trend observed in SRFA. These results highlight the extended elution and greater compositional diversity of coal-derived material relative to SRFA.

Additional results for Suwannee River humic acid (SRHA), Pahokee Peat fulvic acid (PPFA), and coal tar−derived, water-soluble material are presented in Figures S3−S5. SRHA and PPFA show overall trends similar to those of SRFA, with variations in the onset and extent of aromatic fractions. The coal tar−derived material exhibits sustained aromatic dominance throughout the gradient and a gradual increase in oxygen content, consistent with oxidative weathering of PAHs. These results are discussed further in the Supporting Information (Section S2).

Molecular Formula Assignment for Individual Spectra

The data were also analyzed with Python Tools for complex matrices molecular characterization (PyC2MC), a recently developed software package that performs spectrum-by-spectrum calibration and molecular formula assignment across the chromatographic run.[34,35] A walking calibration, based on a master list of peaks obtained from the segmented analysis, provided high mass accuracy and enabled the generation of compositional chromatograms. This approach provided high-resolution tracking of molecular shifts and a detailed view of the compositional changes throughout the elution. Notably, the median mass accuracy for individual-spectra assignments (0.13 ± 0.03 ppm) is comparable to that obtained for segmented analyses (0.12 ± 0.03 ppm) and direct-infusion data (0.14 ± 0.04 ppm), confirming that the individual-spectrum approach maintains an equivalent assignment precision.

Figure 4a shows a representative single-scan mass spectrum of SRFA at 9.3 min, covering the m/z 200−1000 range. From this scan, 3,033 molecular formulas were assigned, accounting for 91.1% of total signal abundance, with an assignment error

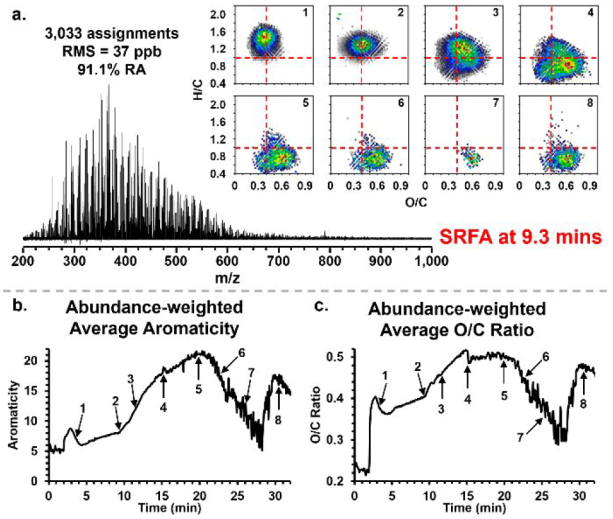

Figure 4. (a) Single-scan mass spectrum of SRFA at 9.3 min with 3,033 assigned formulas. Van Krevelen diagrams show compositional changes across the chromatographic run, labeled by acquisition time. (b) Abundance-weighted aromaticity and (c) O/C ratio chromatograms, calculated from individual spectra using PyC2MC. Numbered points match the spectra shown in panel (a).

of only 37 parts per billion (ppb). This exceptionally low error demonstrates the ultrahigh mass accuracy of 21 T FT-ICR MS, which is essential for HPLC analysis of highly complex mixtures. Van Krevelen diagrams from seven additional time points reveal compositional trends consistent with those observed in the segmented analysis.

From the individual spectra, abundance-weighted features, such as aromaticity and O/C ratios, were calculated and plotted over time (Figure 4b), yielding a compositional chromatogram. Aromaticity, defined as the ratio of abundance-weighted double bond equivalents (DBE) to H/C, reflects molecular unsaturation and condensation. Molecules with high aromaticity typically show elevated DBE and low H/C due to limited CH_2 content, as in condensed structures like coronene. In contrast, low aromaticity corresponds to species with low DBE and high alkylation.

The aromaticity chromatogram shows a baseline of ∼5 before 3 min, corresponding to methanol-soluble compounds. Aromaticity then increases steadily, peaking just after 20 min as more aromatic species elute. A decline between 20−27 min likely reflects background ions commonly observed in negative-ion ESI, such as fatty acids, which ionize efficiently but exhibit low aromaticity and O/C. At 28 min, aromaticity increases again as the gradient shifts from 2 to 5% DEA, releasing the more strongly retained compounds. A local maximum appears near 30 min, just before column reconditioning. These patterns align with the van Krevelen diagrams, which show a shift toward lower H/C ratios.

Importantly, background ions (e.g., m/z = 255, 283, and 410) correspond to persistent contaminants present in blanks and system washes. They remain stable across the chromatographic gradient during blank runs but are partially suppressed during sample analyses when highly ionizable DOM components elute, consistent with competitive ionization effects rather than chromatographically retained background.

The O/C chromatogram follows a similar trend. It starts at ∼0.23 and increases to 0.40 during early elution, followed by a brief dip, and then rises again to a maximum at ∼15 min. A

https://doi.org/10.1021/acs.analchem.5c05562
Anal. Chem. 2026, 98, 601−610

plateau from 15 to 20 min reflects continued elution of oxygen-rich species. The agreement between these trends and the segmented van Krevelen profiles confirms that PyC2MC captures molecular-level changes throughout the chromatographic run.

It is important to highlight that both the segmented (PetroOrg) and individual spectra (PyC2MC) workflows produced consistent compositional trends and comparable mass-accuracy performance (median 0.12−0.15 ppm). PetroOrg maximizes molecular coverage through signal coaddition, whereas PyC2MC increases temporal resolution by tracking molecular variations scan-by-scan. The two methods, therefore, provide complementary views of the same underlying chromatographic behavior.

Furthermore, the consistency between Figures 3 and 4 demonstrates that both the segmented and individual-spectra (PyC2MC) analyses capture the same compositional evolution for the Ox species, characterized by decreasing H/C ratios and increasing O/C.

Comparison of HPLC-MS and DI-MS Analyses

Figure 5 compares molecular formula assignments from segmented HPLC-MS and DI-MS analyses. The first column

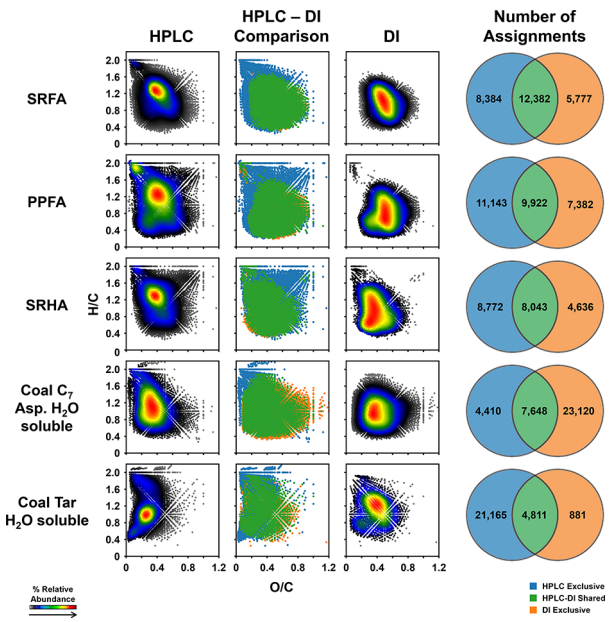

Figure 5. Van Krevelen diagrams from HPLC-MS and DI-MS analyses for each sample type. Center column shows overlapping (green) and exclusive formulas for LC (blue) and DI (orange). Venn diagrams indicate the number of unique and shared molecular formulas per method.

displays the full HPLC-MS data set, the last column shows DI-MS results, and the middle highlights shared and unique formulas. Assignments exclusive to HPLC-MS appear in blue, DI-MS in orange, and those shared in green. HPLC-MS assignments were consolidated across adjacent segments. If a formula appeared in nonadjacent segments separated by more than 10 min, it was counted as a distinct species, indicating potential isomeric diversity. This threshold is supported by the elution behavior of model compounds (Figure 2), where individual peaks span up to ∼10 min, and confirmed isomers (e.g., compounds 6 and 7) elute within overlapping timeframes. A recent study on biooil characterization using the same stationary phase and a similar eluent system also reported isomer separations under 10 min.[36] This conservative cutoff avoids overcounting overlapping isomers while still capturing relevant chromatographic resolution. Figure 5 also presents Venn diagrams summarizing the number of formulas unique to each method and those shared between them.

For SRFA, HPLC-MS revealed a broader molecular formula distribution, with H/C ratios ranging from 0.3 to 2.0 and O/C ratios from 0.1 to 1.0. In contrast, DI-MS covered narrower ranges: H/C from 0.3 to 1.7 and O/C from 0.2 to 0.9. Both methods detected shared formulas concentrated in the central region of the van Krevelen diagram. However, HPLC-MS uniquely captured compounds with lower oxygen and higher hydrogen contents, extending into the saturated, low-oxygen region. By contrast, DI-MS more effectively identified highly oxygenated species (e.g., O_{25-29}), benefiting from the superior signal-to-noise ratio achieved through coaddition of hundreds of transients from a constant-composition sample. These results highlight the complementary strengths of the two methods: HPLC-MS improves detection of less oxygenated, more saturated species, while DI-MS excels at identifying low-abundance, oxygen-rich compounds.

Globally, average O/C, H/C, and m/z values indicate that HPLC-MS preferentially detects more polar, lower-mass species, whereas DI-MS favors slightly more oxygenated, higher-mass compounds. These quantitative differences are modest but systematic, consistent with the compositional overlap shown in Figure 5.

For PPFA, HPLC-MS revealed a broader molecular formula distribution, with distinct gains in the high H/C and low O/C region typical of aliphatic species. DI-MS assignments were concentrated in the central region of the van Krevelen diagram and included unique formulas with moderate and elevated O/C. HPLC-MS also captured additional species in the carbohydrate-like region (high H/C, high O/C), while DI-MS emphasized highly aromatic compounds.

SRHA showed compositional trends similar to those of PPFA. DI-MS produced a more continuous distribution extending from the central region toward the high H/C, low O/C domain of the van Krevelen diagram, consistent with humic material rich in carbon and low in oxygen. In contrast, HPLC-MS provided broader coverage of carbohydrate-like species.

Coal-derived samples exhibited pronounced differences between methods. In the coal tar water-soluble fraction, HPLC-MS uniquely detected species with H/C > 1.6, absent in DI-MS. Consistent with this behavior, coal-asphaltene water-solubles showed additional HPLC-MS formulas in the low O/C, high H/C region, whereas DI-MS favored more oxygen-rich species concentrated in the high O/C domain.

Figure 5 highlights the distinct yet complementary coverage of HPLC-MS and DI-MS across all sample types. For SRFA, most formulas fall within the shared region, reflecting strong compositional agreement. In contrast, PPFA and SRHA show more HPLC-exclusive assignments, particularly at high H/C across a broad O/C range, extending from oxygen-depleted compositions to O/C ≈ 1, consistent with carbohydrate-like species. These patterns indicate that while both techniques capture the core DOM composition, HPLC-MS extends detection into more saturated regions often missed by DI-MS.

In the coal C_7 asphaltene water-soluble fraction, DI-MS produced more exclusive assignments, primarily among highly oxygenated species. In contrast, the coal tar water-soluble

https://doi.org/10.1021/acs.analchem.5c05562
Anal. Chem. 2026, 98, 601−610

sample yielded a substantially larger number of HPLC-exclusive formulas, concentrated in the low O/C, high H/C region. These findings indicate that HPLC-MS offers broader molecular coverage because chromatographic separation reduces ion suppression by distributing analytes over time, minimizing competition for ionization.

Figure S6 further illustrates differences in the oxygen class distributions across samples. For SRFA, PPFA, and coal asphaltene water-solubles, DI-MS profiles are centered around higher oxygen numbers, whereas HPLC-MS shifts toward compounds with lower oxygen content. In SRHA and coal tar samples, HPLC-MS shows flatter and broader distributions, while DI-MS remains narrower and skewed toward more oxidized species. For example, coal tar–derived species span from O_1 to O_{14} in DI-MS, whereas HPLC-MS shows a more even distribution across this range, with increased relative abundance at lower oxygen classes. Highly oxidized samples like SRFA extend to O_{29} in DI-MS. These patterns confirm that HPLC-MS enhances detection of species with low oxygen numbers and expands overall molecular coverage.

CONCLUSIONS

This study demonstrates a method that couples ultrahigh-resolution mass spectrometry with liquid chromatography to improve molecular characterization of DOM from both natural and anthropogenic sources. The method uses a polymeric stationary phase with dimethylaminopropyl functionalities, enabling weak anion exchange and hydrogen-bonding interactions. This retention mechanism offers a functional alternative to conventional C18 chromatography, which relies on hydrophobic interactions and poorly retains polar acidic species. The POROS-based approach improves detection of polyfunctional compounds, particularly hydrogen-rich/low-oxygen species often missing in DI-MS.

PyC2MC enabled spectrum-by-spectrum analysis of the chromatographic run, revealing compositional trends in aromaticity and oxygen content not apparent in DI-MS. While DI-MS provided greater sensitivity for oxygen-rich, low-abundance compounds due to transient coaddition, HPLC-MS broadened coverage of saturated, low-oxygen species, particularly in samples such as PPFA and coal asphaltene water-solubles. DI-MS remained more effective for detecting highly oxidized materials, including coal tar–derived compounds.

The individual spectral approach provides higher temporal resolution, resolving fine compositional changes across the chromatographic run. This increased resolution comes with a moderate trade-off in signal-to-noise ratio and the number of assigned molecular formulas per time segment, as each transient represents a narrower elution window. In contrast, the segmented approach, which coadds multiple transients, enhances mass accuracy and molecular coverage but reduces temporal granularity. Both methods yielded consistent compositional trends. Thus, the optimal strategy depends on the analytical goal. Individual spectra are preferred when temporal resolution and elution dynamics are of interest, whereas segmented spectra are advantageous for comparisons between segments and samples and overall molecular coverage.

The complementary strengths of HPLC-MS and DI-MS provide a more comprehensive view of DOM composition and emerging contaminants. Combined, these approaches enhance molecular coverage and improve confidence in the analysis of complex environmental mixtures.

ASSOCIATED CONTENT

Data Availability Statement

All data can be found in the OSF repository: DOI: 10.17605/OSF.IO/CEV5S.

Supporting Information

The Supporting Information is available free of charge at https://pubs.acs.org/doi/10.1021/acs.analchem.5c05562.

Additional details for experimental methods, tables with compound names, molecular weights, molecular formulas, and additional results (PDF)

AUTHOR INFORMATION

Corresponding Author

Martha L. Aguilera − *National High Magnetic Field Laboratory, Tallahassee, Florida 32310, United States; International Joint Laboratory for Complex Matrices Molecular Characterization, iC2MC, TRTG, Gonfreville 76700 Harfleur, France;* orcid.org/0000-0002-7273-5343; Phone: +1 850-644-1319; Email: maguilera@magnet.fsu.edu

Authors

Joseph W. Frye-Jones − *National High Magnetic Field Laboratory, Tallahassee, Florida 32310, United States; Department of Chemistry and Biochemistry, Florida State University, Tallahassee, Florida 32306, United States;* orcid.org/0000-0003-3618-8052

Lissa C. Anderson − *National High Magnetic Field Laboratory, Tallahassee, Florida 32310, United States; Department of Chemistry and Biochemistry, Florida State University, Tallahassee, Florida 32306, United States;* orcid.org/0000-0001-8633-0251

Winston K. Robbins − *National High Magnetic Field Laboratory, Tallahassee, Florida 32310, United States;* orcid.org/0000-0003-3821-1287

Germain Salvato Vallverdu − *International Joint Laboratory for Complex Matrices Molecular Characterization, iC2MC, TRTG, Gonfreville 76700 Harfleur, France; E2S UPPA, CNRS, IPREM, Université de Pau et des Pays de l'Adour, UMR 5254, 64053 Pau, France;* orcid.org/0000-0003-1116-8776

Alvaro J. Tello Rodriguez − *National High Magnetic Field Laboratory, Tallahassee, Florida 32310, United States*

Mason C. Hagan − *National High Magnetic Field Laboratory, Tallahassee, Florida 32310, United States*

[#]Alan G. Marshall − *National High Magnetic Field Laboratory, Tallahassee, Florida 32310, United States; Department of Chemistry and Biochemistry, Florida State University, Tallahassee, Florida 32306, United States;* orcid.org/0000-0001-9375-2532

Brice Bouyssiere − *International Joint Laboratory for Complex Matrices Molecular Characterization, iC2MC, TRTG, Gonfreville 76700 Harfleur, France; E2S UPPA, CNRS, IPREM, Université de Pau et des Pays de l'Adour, UMR 5254, 64053 Pau, France;* orcid.org/0000-0001-5878-6067

Pierre Giusti − *International Joint Laboratory for Complex Matrices Molecular Characterization, iC2MC, TRTG, Gonfreville 76700 Harfleur, France; Total Energies Refining and Chemicals, Total Research and Technology, Gonfreville*

76700 Harfleur, France; orcid.org/0000-0002-9569-3158

Ryan P. Rodgers − *National High Magnetic Field Laboratory, Tallahassee, Florida 32310, United States; Department of Chemistry and Biochemistry, Florida State University, Tallahassee, Florida 32306, United States; International Joint Laboratory for Complex Matrices Molecular Characterization, iC2MC, TRTG, Gonfreville 76700 Harfleur, France; E2S UPPA, CNRS, IPREM, Université de Pau et des Pays de l'Adour, UMR 5254, 64053 Pau, France;* orcid.org/0000-0003-1302-2850

Complete contact information is available at: https://pubs.acs.org/10.1021/acs.analchem.5c05562

Author Contributions

All authors contributed to the manuscript and approved the final version.

Notes

The authors declare no competing financial interest.
#AGM Deceased on June 6, 2025.

■ ACKNOWLEDGMENTS

This work was conducted at the National High Magnetic Field Laboratory Ion Cyclotron Resonance User Facility, supported by NSF Division of Chemistry (DMR-2128556) and the State of Florida.

■ REFERENCES

(1) Moran, M. A.; Zepp, R. G. Role of Photoreactions in the Formation of Biologically Labile Compounds from Dissolved Organic Matter. *Limnol Oceanogr* **1997**, *42* (6), 1307−1316.
(2) Battin, T. J.; Luyssaert, S.; Kaplan, L. A.; Aufdenkampe, A. K.; Richter, A.; Tranvik, L. J. The Boundless Carbon Cycle. *Nat. Geosci* **2009**, *2* (9), 598−600.
(3) Regnier, P.; Resplandy, L.; Najjar, R. G.; Ciais, P. The Land-to-Ocean Loops of the Global Carbon Cycle. *Nature* **2022**, *603* (7901), 401−410.
(4) Niles, S. F.; Chacón-Patiño, M. L.; Chen, H.; McKenna, A. M.; Blakney, G. T.; Rodgers, R. P.; Marshall, A. G. Molecular-Level Characterization of Oil-Soluble Ketone/Aldehyde Photo-Oxidation Products by Fourier Transform Ion Cyclotron Resonance Mass Spectrometry Reveals Similarity between Microcosm and Field Samples. *Environ. Sci. Technol.* **2019**, *53* (12), 6887−6894.
(5) Freeman, D. H.; Nelson, R. K.; Pate, K.; Reddy, C. M.; Ward, C. P. Forecasting Photo-Dissolution for Future Oil Spills at Sea: Effects of Oil Properties and Composition. *Environ. Sci. Technol.* **2024**, *58* (34), 15236−15245.
(6) Glattke, T. J.; Chacón-Patiño, M. L.; Hoque, S. S.; Ennis, T. E.; Greason, S.; Marshall, A. G.; Rodgers, R. P. Complex Mixture Analysis of Emerging Contaminants Generated from Coal Tar- and Petroleum-Derived Pavement Sealants: Molecular Compositions and Correlations with Toxicity Revealed by Fourier Transform Ion Cyclotron Resonance Mass Spectrometry. *Environ. Sci. Technol.* **2022**, *56* (18), 12988−12998.
(7) Glattke, T. J.; Chacón-Patiño, M. L.; Marshall, A. G.; Rodgers, R. P. Maltene and Asphaltene Contributions to the Formation of Water-Soluble Emerging Contaminants from Photooxidation of Paving Materials. *Energy Fuels* **2022**, *36* (21), 13060−13072.
(8) Kujawinski, E. B.; Hatcher, P. G.; Freitas, M. A. High-Resolution Fourier Transform Ion Cyclotron Resonance Mass Spectrometry of Humic and Fulvic Acids: Improvements and Comparisons. *Anal. Chem.* **2002**, *74* (2), 413−419.
(9) Koch, B. P.; Dittmar, T. From Mass to Structure: An Aromaticity Index for High-Resolution Mass Data of Natural Organic Matter. *Rapid Commun. Mass Spectrom.* **2006**, *20* (5), 926−932.
(10) Mopper, K.; Stubbins, A.; Ritchie, J. D.; Bialk, H. M.; Hatcher, P. G. Advanced Instrumental Approaches for Characterization of Marine Dissolved Organic Matter: Extraction Techniques, Mass Spectrometry, and Nuclear Magnetic Resonance Spectroscopy. *Chem. Rev.* **2007**, *107* (2), 419−442.
(11) Minor, E. C.; Steinbring, C. J.; Longnecker, K.; Kujawinski, E. B. Characterization of Dissolved Organic Matter in Lake Superior and Its Watershed Using Ultrahigh Resolution Mass Spectrometry. *Org. Geochem.* **2012**, *43*, 1−11.
(12) Kellerman, A. M.; Dittmar, T.; Kothawala, D. N.; Tranvik, L. J. Chemodiversity of Dissolved Organic Matter in Lakes Driven by Climate and Hydrology. *Nat. Commun.* **2014**, *5* (1), 3804.
(13) Bahureksa, W.; Borch, T.; Young, R. B.; Weisbrod, C. R.; Blakney, G. T.; McKenna, A. M. Improved Dynamic Range, Resolving Power, and Sensitivity Achievable with FT-ICR Mass Spectrometry at 21 T Reveals the Hidden Complexity of Natural Organic Matter. *Anal. Chem.* **2022**, *94* (32), 11382−11389.
(14) Rodgers, R. P.; Mapolelo, M. M.; Robbins, W. K.; Chacón-Patiño, M. L.; Putman, J. C.; Niles, S. F.; Rowland, S. M.; Marshall, A. G. Combating Selective Ionization in the High Resolution Mass Spectral Characterization of Complex Mixtures. *Faraday Discuss.* **2019**, *218*, 29−51.
(15) Rowland, S. M.; Robbins, W. K.; Corilo, Y. E.; Marshall, A. G.; Rodgers, R. P. Solid-Phase Extraction Fractionation to Extend the Characterization of Naphthenic Acids in Crude Oil by Electrospray Ionization Fourier Transform Ion Cyclotron Resonance Mass Spectrometry. *Energy Fuels* **2014**, *28* (8), 5043−5048.
(16) Clingenpeel, A. C.; Rowland, S. M.; Corilo, Y. E.; Zito, P.; Rodgers, R. P. Fractionation of Interfacial Material Reveals a Continuum of Acidic Species That Contribute to Stable Emulsion Formation. *Energy Fuels* **2017**, *31* (6), 5933−5939.
(17) Lobodin, V. V.; Robbins, W. K.; Lu, J.; Rodgers, R. P. Separation and Characterization of Reactive and Non-Reactive Sulfur in Petroleum and Its Fractions. *Energy Fuels* **2015**, *29* (10), 6177−6186.
(18) Rowland, S. M.; Smith, D. F.; Blakney, G. T.; Corilo, Y. E.; Hendrickson, C. L.; Rodgers, R. P. Online Coupling of Liquid Chromatography with Fourier Transform Ion Cyclotron Resonance Mass Spectrometry at 21 T Provides Fast and Unique Insight into Crude Oil Composition. *Anal. Chem.* **2021**, *93* (41), 13749−13754.
(19) Patrone, J.; Vila-Costa, M.; Dachs, J.; Papazian, S.; Gago-Ferrero, P.; Gil-Solsona, R. Enhancing Molecular Characterization of Dissolved Organic Matter by Integrative Direct Infusion and Liquid Chromatography Nontargeted Workflows. *Environ. Sci. Technol.* **2024**, *58* (28), 12454−12466.
(20) Patriarca, C.; Bergquist, J.; Sjöberg, P. J. R.; Tranvik, L.; Hawkes, J. A. Online HPLC-ESI-HRMS Method for the Analysis and Comparison of Different Dissolved Organic Matter Samples. *Environ. Sci. Technol.* **2018**, *52* (4), 2091−2099.
(21) Boiteau, R. M.; Corilo, Y. E.; Kew, W. R.; Dewey, C.; Alvarez Rodriguez, M. C.; Carlson, C. A.; Conway, T. M. Relating Molecular Properties to the Persistence of Marine Dissolved Organic Matter with Liquid Chromatography−Ultrahigh-Resolution Mass Spectrometry. *Environ. Sci. Technol.* **2024**, *58* (7), 3267−3277.
(22) Frye-Jones, J. W.; Chacón-Patiño, M. L.; Anderson, L. C.; Tello-Rodriguez, A. J.; Robbins, W. K.; Marshall, A. G.; Rodgers, R. P. *Expanding Molecular Compositional Coverage of Water-Soluble Emerging Contaminants with Liquid Chromatography- Ultrahigh-Resolution Mass Spectrometry*; American Society of Mass Spectrometry: Anaheim, 2024.
(23) Hendrickson, C. L.; Quinn, J. P.; Kaiser, N. K.; Smith, D. F.; Blakney, G. T.; Chen, T.; Marshall, A. G.; Weisbrod, C. R.; Beu, S. C. 21 T Fourier Transform Ion Cyclotron Resonance Mass Spectrometer: A National Resource for Ultrahigh Resolution Mass Analysis. *J. Am. Soc. Mass Spectrom.* **2015**, *26* (9), 1626−1632.
(24) Corilo, Y. E. *PetroOrg*; Omics, LLC: Tallahassee, FL, 2014. https://nationalmaglab.org/user-facilities/icr/software/.

(25) Blakney, G. T.; Hendrickson, C. L.; Marshall, A. G. Predator Data Station: A Fast Data Acquisition System for Advanced FT-ICR MS Experiments. *Int. J. Mass Spectrom.* **2011**, *306* (2−3), 246−252.
(26) Sueur, M.; Maillard, J. F.; Lacroix-Andrivet, O.; Rüger, C. P.; Giusti, P.; Lavanant, H.; Afonso, C. PyC2MC: An Open-Source Software Solution for Visualization and Treatment of High-Resolution Mass Spectrometry Data. *J. Am. Soc. Mass Spectrom.* **2023**, *34* (4), 617−626.
(27) Frye-Jones, J. W.; Chacón-Patiño, M. L.; Marshall, A. G.; Rodgers, R. P. Photoinduced Oxidation and Polymerization in Oil-Soluble Products and Interfacial Material from Petroleum Weathering. *Energy Fuels* **2025**, *39* (2), 1031−1041.
(28) Rodgers, R. P.; Chacon-Patino, M. L.; Robbins, W. K.; Giraldo, D.; Frye-Jones, J. W.; Weisbrod, C.; Marshall, A. G.; Bouyssiere, B.; Giusti, P. *Online LC/21T FT-ICR MS and ICP-MS Analysis of Dissolved Organic Matter (DOM). In 71st ASMS Conference on Mass Spectrometry and Allied Topics*; American Society of Mass Spectrometry: Houston, 2023.
(29) Putman, J. C.; Moulian, R.; Smith, D. F.; Weisbrod, C. R.; Chacon-Patino, M. L.; Corilo, Y. E.; Blakney, G. T.; Rumancik, L. E.; Barrere-Mangote, C.; Rodgers, R. P.; Giusti, P.; Marshall, A. G.; Bouyssiere, B. Probing Aggregation Tendencies in Asphaltenes by Gel Permeation Chromatography. Part 2: Online Detection by Fourier Transform Ion Cyclotron Resonance Mass Spectrometry and Inductively Coupled Plasma Mass Spectrometry. *Energy Fuels* **2020**, *34* (9), 10915−10925.
(30) McKenna, A. M.; Chacón-Patiño, M. L.; Chen, H.; Blakney, G. T.; Mentink-Vigier, F.; Young, R. B.; Ippolito, J. A.; Borch, T. Expanding the Analytical Window for Biochar Speciation: Molecular Comparison of Solvent Extraction and Water-Soluble Fractions of Biochar by FT-ICR Mass Spectrometry. *Anal. Chem.* **2021**, *93* (46), 15365−15372.
(31) Glattke, T. J.; Chacón-Patiño, M. L.; Marshall, A. G.; Rodgers, R. P. Molecular Characterization of Photochemically Produced Asphaltenes via Photooxidation of Deasphalted Crude Oils. *Energy Fuels* **2020**, *34* (11), 14419−14428.
(32) Henriksen, T.; Juhler, R. K.; Svensmark, B.; Cech, N. B. The Relative Influences of Acidity and Polarity on Responsiveness of Small Organic Molecules to Analysis with Negative Ion Electrospray Ionization Mass Spectrometry (ESI-MS). *J. Am. Soc. Mass Spectrom.* **2005**, *16* (4), 446−455.
(33) Cech, N. B.; Enke, C. G. Practical Implications of Some Recent Studies in Electrospray Ionization Fundamentals. *Mass Spectrom Rev.* **2001**, *20* (6), 362−387.
(34) Salvato Vallverdu, G.; Celis Cornejo, C.; Chacón-Patiño, M. L.; Rüger, C. P.; Maillard, J.; Afonso, C.; Hendrickson, C. L.; Bouyssiere, B.; Giusti, P.; Rodgers, R. P. *PyC2MC: A Novel Software Platform for the Automated Analysis of LC-HRMS Data of Complex Mixtures*; American Society of Mass Spectrometry: Baltimore, 2025.
(35) Sueur, M.; Salvato Vallverdu, G.; Maillard, J.; Rüger, C. P.; Tello Rodriguez, A. J.; Chacon-Patino, M. L.; Bouyssiere, B.; Rodgers, R. P.; Giusti, P.; Afonso, C. *PyC2MC: A Workflow-Driven Framework for FTMS Data Processing and Molecular Attribution*; American Society of Mass Spectrometry: Baltimore, 2025.
(36) Chacón-Patiño, M. L.; Frye-Jones, J. W.; Anderson, L. C.; Robbins, W. K.; Salvato Vallverdu, G.; Tello-Rodríguez, Á. J.; Ruiz, W.; Gascon, G.; Rüger, C. P.; Dayton, D. C.; Giusti, P.; Mase, C.; Barrère-Mangote, C.; Afonso, C.; Bouyssiere, B.; Rodgers, R. P. Detailed Molecular Composition of Wood Pyrolysis Bio-Oils Revealed by HPLC-FT-ICR MS. *Energy Fuels* **2025**, *39* (7), 3575−3588.

https://doi.org/10.1021/acs.analchem.5c05562
Anal. Chem. 2026, 98, 601−610